CRYSTAL GROWTH & DESIGN

pubs.acs.org/crystal

Communication

# Enhancing Single-Crystal Dichroism of an Asymmetric Azo Chromophore by Perfluorophenyl Embraces and Boron Coordination

Gonzalo Campillo-Alvarado,* Rachel J. Liu, Daniel W. Davies, and Ying Diao

Cite This: https://doi.org/10.1021/acs.cgd.1c00114

Read Online

ACCESS | Metrics & More | Article Recommendations | Supporting Information

**ABSTRACT:** We describe the use of perfluorophenyl embraces and boron coordination (B ← N) to enhance dichroism in single crystals of an asymmetric azo chromophore. Specifically, a tripod-shaped boron adduct comprised of tris(pentafluorophenyl)borane (**BCF**) and 4-phenylazopyridine (**4PAzP**) self-assembles as supramolecular helices through perfluorophenyl embraces, wherein the azo chromophores are aligned in parallel through B ← N bonds. The alignment of molecular transition dipole moments in (**BCF**)·(**4PAzP**) results in enhanced dichroism compared to pure **4PAzP** as confirmed by polarized optical microscopy. The study offers a novel supramolecular strategy to enhance dichroism in single-crystalline materials.

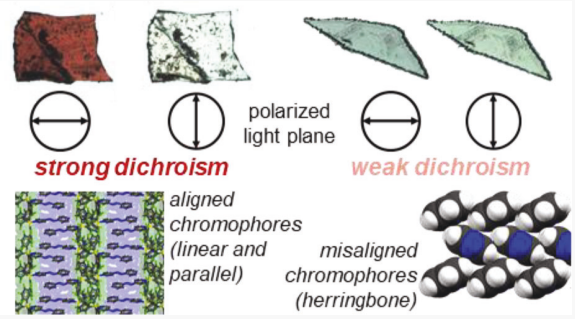


The ability to fine-tune light−matter interactions has experienced sustained development in the chemical and physical sciences. Particularly, linear dichroism (i.e., difference in absorption of light linearly polarized dependent on the orientation axis)[1] in anisotropic materials has been exploited in diverse fields, including nanomachines,[2,3] metal−organic frameworks,[4] films,[5−7] wave optics,[8] photodetection,[9,10] imaging,[11,12] and polarizer development.[1,13,14] Although dichroic single crystals have been widely documented,[15−23] strategies to engineer and modulate dichroism in organic crystals have remained relatively underexplored.

Pioneering work of dichroism engineering in single crystals by Friščić and Barrett et al. involved exploiting halogen bonding[24−26] to align azobenzene (azo) chromophores in cocrystals. Specifically, alignment of transition dipole moments of chromophores resulted in strong dichroism, wherein the absorption of plane-polarized light is dependent upon its orientation with the crystalline material. While halogen bonding has been effectively used to generate dichroic crystals by overcoming the tendency of azo chromophore materials to pack as a herringbone,[27,28] we envisage additional weak and directional supramolecular interactions in the crystal engineering toolbox can be exploited to align azo chromophores and generate dichroic responses.

Herein, we introduce the ability of perfluorophenyl embraces and boron coordination to generate highly dichroic single crystals. Specifically, the asymmetric azo chromophore 4-phenylazopyridine (**4PAzP**) coordinates orthogonally to tris(pentafluorophenyl)borane (**BCF**) to achieve the formation of a tripod-shaped boron adduct (**BCF**)·(**4PAzP**) (Scheme 1a,b). The adduct (**BCF**)·(**4PAzP**) self-assembles into molecular helices (Scheme 1c) sustained by a combination of perfluorophenyl embraces[29,30] and boron coordination[31−38] in the crystalline solid state where the molecular transition dipole moment from the chromophore is oriented in parallel and therefore generates dichroic behavior (Scheme 1d−f). To the best of our knowledge, there are no documented examples of dichroism enhancement of an asymmetric azo chromophore (i.e., **4PAzP**) and the application of perfluorophenyl embraces and/or boron coordination to achieve dichroism.

As a pure solid, **4PAzP** packs predominantly as a herringbone (herringbone angle, $\theta_H$ = 54.6°), causing a weak dichroic behavior in single crystals due to increased material isotropy (i.e., misalignment of the molecular transition dipole moment of the chromophores) (Figure 1a,b).[24,28]

Our strategy to enhance dichroism of azo chromophore **4PAzP** involved the combination of **4PAzP** (8.26 mg, 0.045 mmol) and **BCF** (23.1 mg, 0.045 mmol) in warm chlorobenzene (3 mL). The solution was heated until all the components dissolved. Single crystals of (**BCF**)·(**4PAzP**) in the form of dark red tablets were obtained through slow evaporation after a period of 5 days.

Single-crystal X-ray diffraction analysis (Tables S1 and S2, Supporting Information) revealed the components of (**BCF**)·

**Received:** January 30, 2021
**Revised:** April 16, 2021

**Scheme 1.** (a) Molecular Structures of BCF, 4PAzP, and (b) Tripod-Shaped Adduct (BCF)·(4PAzP) Displaying the Chromophore Principal Transition Dipole Moment, (c) Cartoon of Molecular Helices in (BCF)·(4PAzP), (d) Representation of Dichroic Response of Single Crystals of (BCF)·(4PAzP) to Mutually Perpendicular Orientations of the Polarizer (i.e., 0° to 90°), and (e, f) Drawings of Main Supramolecular Interactions in This Study: Boron Coordination and Perfluorophenyl Embrace

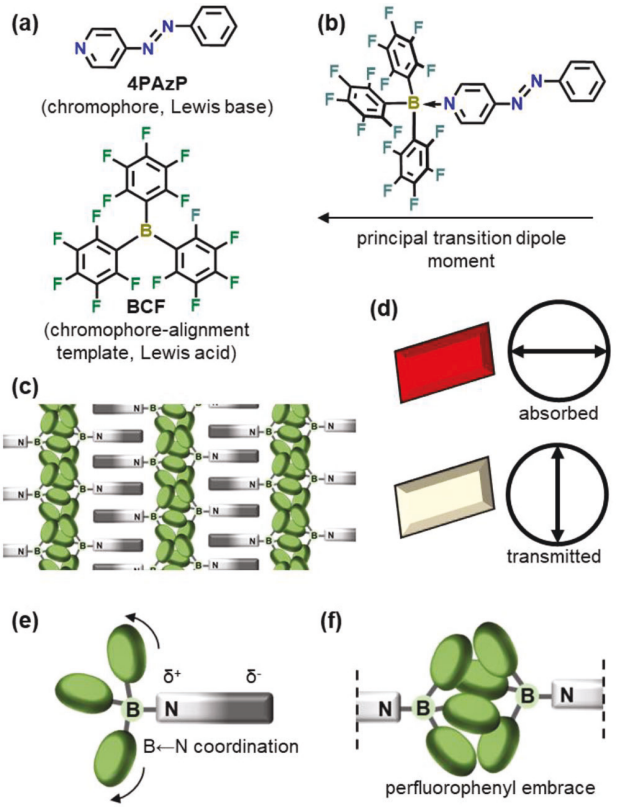


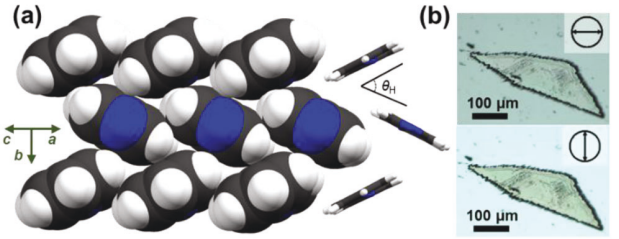


**Figure 1.** (a) Crystal structures of pure **4PAzP** showing a herringbone packing arrangement (CSD refcode: QUFDIG)[28] and (b) photographs of weakly dichroic single crystals of **4PAzP** viewed under polarized light in mutually perpendicular orientations.

(**4PAzP**) to crystallize in the monoclinic space group $P2_1/n$. In the solid, **BCF** interacts with the azo chromophore **4PAzP** through B ← N bonds (1.621(2) and 1.622(2) Å) as two crystallographically independent adducts of (**BCF**)·(**4PAzP**) in the asymmetric unit. The adducts are sustained by face-to-face [$\pi\cdots\pi$] stacking (Figure 2a) in a head-to-head geometry. **BCF** undergoes a change in geometry from trigonal planar[39] to tetrahedral.[31,33,40] The B ← N bonds are slightly weaker compared to similar adducts,[31,32,34] as evidenced by the tetrahedral characters (THC)[41] of 67.2 and 69.8%. The

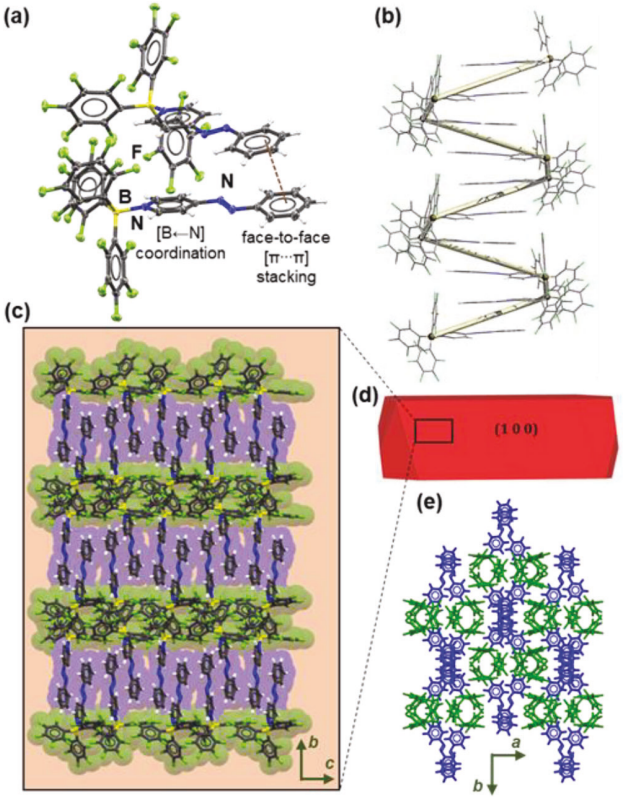


**Figure 2.** Crystal structure of (**BCF**)·(**4PAzP**). (a) Asymmetric unit consisting of two independent adducts. (b) Supramolecular helices where boron atoms serve as nodes. (c) Extended packing showing the linear alignment of chromophores to be parallel with the *b*-axis. (d) Major face of single-crystal BFDH morphology (100). (e) Extended packing showing **BCF** molecules serving as an underpinning for the alignment of **4PAzP** chromophores.

chromophore **4PAzP** adopts a closely planar conformation (dihedral angles: 13.6° and 5.0°), wherein -C−N═N−C- torsion angles are 179.9° and 178.4°. **BCF** lies approximately orthogonal (76.2° and 80.0°) to the pyridyl rings of **4PAzP**. The coordinated adducts (**BCF**)·(**4PAzP**) adopt an overall tripod-shaped geometry where perfluorophenyl rings in **BCF** act as the legs and chromophores **4PAzP** serve as the center columns. The stacked adducts of (**BCF**)·(**4PAzP**), as related by an inversion center, pack into an overall helical architecture (Figure 2b)[42] that runs along the *c*-axis. A combination of perfluorophenyl embraces[29] of the **BCF** fragments containing [C−F···$\pi$] and [F···F] contacts sustain close-packed columns (Figure 2c) that serve as the underpinning for the helices, as well as the linear and parallel arrangement of **4PAzP** chromophores and transition dipole moments in the crystallographic (100) face (Figure 2d,e). The parallel arrangement of chromophores facilitated by **BCF** serves as the condition to achieve single-crystal dichroism.

Dichroism in single crystals of (**BCF**)·(**4PAzP**) was realized by polarized optical microscopy (POM). Specifically, single crystals in a batch of (**BCF**)·(**4PAzP**) changed color from dark red to colorless upon rotation of the polarizer (Figure 3a, Video S1, Supporting Information). The dichroism in crystals of (**BCF**)·(**4PAzP**) was significantly stronger compared to pure crystals of **4PAzP**. To gain further understanding, changes in color and transmitted light intensities in a selected single


https://doi.org/10.1021/acs.cgd.1c00114
Cryst. Growth Des. XXXX, XXX, XXX−XXX

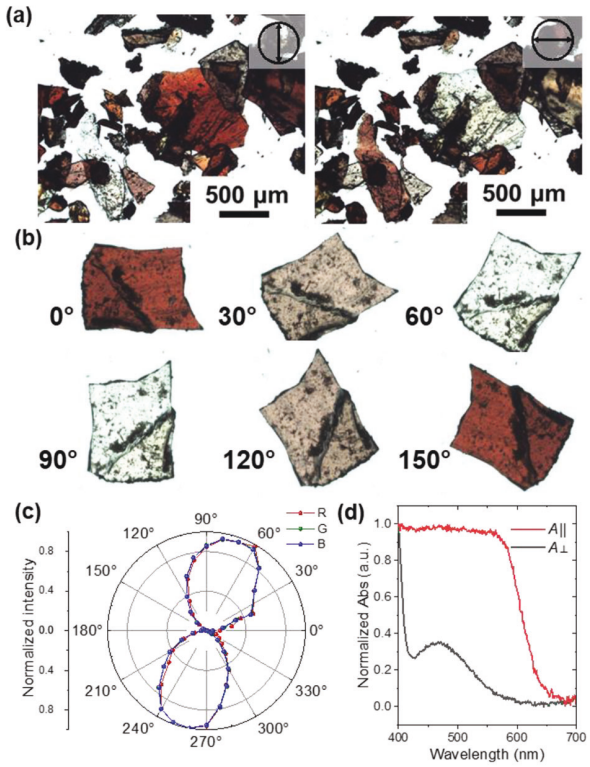


**Figure 3.** (a) Batch of single crystals of (**BCF**)·(**4PAzP**) observed using POM under mutually perpendicular planes of polarized light. (b) A single crystal of (**BCF**)·(**4PAzP**) (100) face observed using POM and consecutively rotating the specimen 30° in relation to the plane of polarized light. (c) Polar plot of transmitted RGB intensities as a function of the orientation of polarized light through the (100) face of (**BCF**)·(**4PAzP**). (d) Normalized absorption spectra of polarized UV−vis spectroscopy with the plane of polarized light directed either parallel (*A*||, red line) or perpendicular (*A*⊥, black line) to the main axis of a single crystal of (**BCF**)·(**4PAzP**).

crystal of (**BCF**)·(**4PAzP**) (100 face) were recorded every 10° of rotation using a rotating stage (Figure 3b, Video S2, Supporting Information). A polar plot of the transmittance of the red, green, and blue (RGB) intensities observed under POM confirmed the anisotropic behavior in single crystals of (**BCF**)·(**4PAzP**) with respect to the plane of polarized light (Figure 3c). Polarized UV−vis spectroscopy of the single-crystal specimen supported the anisotropic absorption that results in dichroic behavior at mutually perpendicular polarized light angles (Figure 3d). Namely, a dark red coloration in single crystals is visible when the transition dipole moments are aligned in parallel with the plane of polarized light (i.e., stronger absorption; see Figures S8, S12, Supporting Information) versus colorless when aligned perpendicularly. The crystals of (**BCF**)·(**4PAzP**) show a strong dichroic ratio, *R*, of 39.22 at 605 nm (see Figure S13, Supporting Information).[43] Further thermal analysis of (**BCF**)·(**4PAzP**) using a heating stage (Linkam Scientific) showed no changes in coloration or crystal shape below the melting temperature at 280 °C (see Figure S7, Supporting Information).

Hirshfeld surface analysis[44−47] of (**BCF**)·(**4PAzP**) revealed the dominant influence of perfluorophenyl embraces[29] in the crystal packing and formation of supramolecular helices. Specifically, fingerprint plots of intermolecular interactions showed that [F···H], [F···F], and [F···C] account for 85.2% of the full interaction map. In contrast, face-to-face and face-to-edge [$\pi\cdots\pi$] stacking (i.e., [C···H] and [C···C]) account for only 8.3% (see Figure S4, Supporting Information). This observation is in agreement with Hartree−Fock calculations using the 3-21G basis set with X-ray coordinates of (**BCF**)·(**4PAzP**). Molecular electrostatic potential surfaces support that the **BCF** motif withdraws electron density from **4PAzP**, becoming negatively charged and a suitable hydrogen bond acceptor. The **4PAzP** chromophore becomes electron-deficient on the pyridyl ring and remains relatively electron-rich on the phenyl ring, thus facilitating the formation of complementary $\pi$-stacking and supramolecular helices.

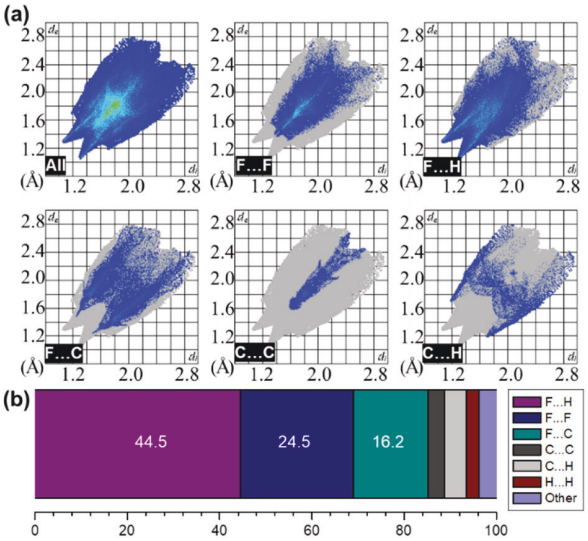


**Figure 4.** (a) Two-dimensional fingerprint plots of interactions in (**BCF**)·(**4PAzP**). (b) Relative contributions to the Hirshfield surface area for close intermolecular contacts in adduct (**BCF**)·(**4PAzP**).

In this work, we have demonstrated the ability of **BCF** to align the molecular transition dipole moments of an asymmetric chromophore (i.e., **4PAzP**) through supramolecular interactions. Namely, a combination of perfluorophenyl embraces and boron coordination in adduct (**BCF**)·(**4PAzP**) promoted the formation of supramolecular helices wherein the main dipole moments of **4PAzP** molecules are linearly oriented, thus generating a strong dichroic response under polarized light. We are currently investigating advanced applications of dichroism such as thin film development and dichroic organic semiconductors. We envisage that control of dichroism in single-crystalline materials could be implemented in multifunctional beam splitters with applications in optoelectronic materials.

## ■ ASSOCIATED CONTENT

### Supporting Information

The Supporting Information is available free of charge at https://pubs.acs.org/doi/10.1021/acs.cgd.1c00114.

Experimental information (materials, instrumentation, and computational methods), single-crystal X-ray diffraction data, polarized optical microscopy data, computational details, and UV−vis spectroscopy data (PDF)


https://doi.org/10.1021/acs.cgd.1c00114
Cryst. Growth Des. XXXX, XXX, XXX−XXX

Polarized optical microscopy observation of dichroism of a batch of single crystals of (**BCF**)·(**4PAzP**) in response to rotation of the polarizer (AVI)

Polarized optical microscopy observation of dichroism of a single crystal of (**BCF**)·(**4PAzP**) in relation to a 360° rotation of the specimen in relation to the plane of polarized light (AVI)

### Accession Codes

CCDC 2058290 (for (**BCF**)·(**4PAzP**)) contains the supplementary crystallographic data for this paper. These data can be obtained free of charge via www.ccdc.cam.ac.uk/data_request/cif, or by emailing data_request@ccdc.cam.ac.uk, or by contacting The Cambridge Crystallographic Data Centre, 12 Union Road, Cambridge CB2 1EZ, UK; fax: +44 1223 336033.

## ■ AUTHOR INFORMATION


### Corresponding Author

**Gonzalo Campillo-Alvarado** − *Department of Chemical and Biomolecular Engineering, University of Illinois Urbana-Champaign, Urbana, Illinois 61801, United States;* orcid.org/0000-0002-1868-8523; Email: gcampi@illinois.edu

### Authors

**Rachel J. Liu** − *Department of Chemical and Biomolecular Engineering, University of Illinois Urbana-Champaign, Urbana, Illinois 61801, United States;* orcid.org/0000-0003-0184-7636

**Daniel W. Davies** − *Department of Chemical and Biomolecular Engineering, University of Illinois Urbana-Champaign, Urbana, Illinois 61801, United States;* orcid.org/0000-0001-5170-4559

**Ying Diao** − *Department of Chemical and Biomolecular Engineering, University of Illinois Urbana-Champaign, Urbana, Illinois 61801, United States;* orcid.org/0000-0002-8984-0051

Complete contact information is available at: https://pubs.acs.org/10.1021/acs.cgd.1c00114


### Notes

The authors declare no competing financial interest.

## ■ ACKNOWLEDGMENTS

G.C.-A. acknowledges financial support from The Office for Access and Equity, the DRIVE Committee, and the Illinois Materials Research Center (University of Illinois at Urbana-Champaign) through the DRIVE Distinguished Postdoctoral Fellowship. G.C.-A. and Y.D. acknowledge partial support by the NSF MRSEC: Illinois Materials Research Center under Grant No. DMR 17-20633. Y.D. and D.W.D. acknowledge the Sloan Foundation for a Sloan Research Fellowship in Chemistry and a 3M Nontenured Faculty Award. We thank Dr. Danielle Gray and Dr. Toby J. Woods for help with single-crystal X-ray diffraction experiments and for helpful discussions. This work was conducted in part in the George L. Clark X-ray Facility and 3M Materials Laboratory.

## ■ REFERENCES


(1) Rodger, A.; Nordén, B. *Circular Dichroism and Linear Dichroism*; Oxford University Press: USA, 1997; Vol. *1*.

(2) Zhan, X.; Zheng, J.; Zhao, Y.; Zhu, B.; Cheng, R.; Wang, J.; Liu, J.; Tang, J.; Tang, J. From Strong Dichroic Nanomotor to Polarotactic Microswimmer. *Adv. Mater.* **2019**, *31*, 1903329.

(3) Martella, D.; Nocentini, S.; Micheletti, F.; Wiersma, D. S.; Parmeggiani, C. Polarization-dependent deformation in light responsive polymers doped by dichroic dyes. *Soft Matter* **2019**, *15*, 1312−1318.

(4) Walton, I. M.; Cox, J. M.; Coppin, J. A.; Linderman, C. M.; Patel, D. G. D.; Benedict, J. B. Photo-responsive MOFs: light-induced switching of porous single crystals containing a photochromic diarylethene. *Chem. Commun.* **2013**, *49*, 8012−8014.

(5) Park, G.; Choi, Y.-S.; Yun, H. S.; Yoon, D. K. Fabrication of bilayer dichroic films using liquid crystal materials for multiplex applications. *ACS Appl. Mater. Interfaces* **2020**, *12*, 45315−45321.

(6) Park, K. S.; Kwok, J. J.; Dilmurat, R.; Qu, G.; Kafle, P.; Luo, X.; Jung, S.-H.; Olivier, Y.; Lee, J.-K.; Mei, J.; Beljonne, D.; Diao, Y. Tuning conformation, assembly, and charge transport properties of conjugated polymers by printing flow. *Sci. Adv.* **2019**, *5*, No. eaaw7757.

(7) Mohammadi, E.; Zhao, C.; Meng, Y.; Qu, G.; Zhang, F.; Zhao, X.; Mei, J.; Zuo, J.-M.; Shukla, D.; Diao, Y. Dynamic-template-directed multiscale assembly for large-area coating of highly-aligned conjugated polymer thin films. *Nat. Commun.* **2017**, *8*, 16070.

(8) Qiao, J.; Kong, X.; Hu, Z.-X.; Yang, F.; Ji, W. High-mobility transport anisotropy and linear dichroism in few-layer black phosphorus. *Nat. Commun.* **2014**, *5*, 4475.

(9) Liu, F.; Zheng, S.; He, X.; Chaturvedi, A.; He, J.; Chow, W. L.; Mion, T. R.; Wang, X.; Zhou, J.; Fu, Q.; Fan, H. J.; Tay, B. K.; Song, L.; He, R.-H.; Kloc, C.; Ajayan, P. M.; Liu, Z. Highly Sensitive Detection of Polarized Light Using Anisotropic 2D ReS2. *Adv. Funct. Mater.* **2016**, *26*, 1169−1177.

(10) Li, M.; Han, S.; Teng, B.; Li, Y.; Liu, Y.; Liu, X.; Luo, J.; Hong, M.; Sun, Z. Minute-Scale Rapid Crystallization of a Highly Dichroic 2D Hybrid Perovskite Crystal toward Efficient Polarization-Sensitive Photodetector. *Adv. Opt. Mater.* **2020**, *8*, 2000149.

(11) Jin, L.-W.; Claborn, K. A.; Kurimoto, M.; Geday, M. A.; Maezawa, I.; Sohraby, F.; Estrada, M.; Kaminksy, W.; Kahr, B. Imaging linear birefringence and dichroism in cerebral amyloid pathologies. *Proc. Natl. Acad. Sci. U. S. A.* **2003**, *100*, 15294−15298.

(12) Martínez-Martínez, V.; Corcóstegui, C.; Prieto, J. B.; Gartzia, L.; Salleres, S.; Arbeloa, I. L. Distribution and orientation study of dyes intercalated into single sepiolite fibers. A confocal fluorescence microscopy approach. *J. Mater. Chem.* **2011**, *21*, 269−276.

(13) Nordén, B. Applications of linear dichroism spectroscopy. *Appl. Spectrosc. Rev.* **1978**, *14*, 157−248.

(14) Pan, S.; Ho, J. Y.; Chigrinov, V. G.; Kwok, H. S. Novel Photoalignment Method Based on Low-Molecular-Weight Azobenzene Dyes and Its Application for High-Dichroic-Ratio Polarizers. *ACS Appl. Mater. Interfaces* **2018**, *10*, 9032−9037.

(15) Kaminsky, W.; Claborn, K.; Kahr, B. Polarimetric imaging of crystals. *Chem. Soc. Rev.* **2004**, *33*, 514−525.

(16) Zhou, Z.; Long, M.; Pan, L.; Wang, X.; Zhong, M.; Blei, M.; Wang, J.; Fang, J.; Tongay, S.; Hu, W.; Li, J.; Wei, Z. Perpendicular Optical Reversal of the Linear Dichroism and Polarized Photodetection in 2D GeAs. *ACS Nano* **2018**, *12*, 12416−12423.

(17) Liu, H.; Lu, Z.; Tang, B.; Qu, C.; Zhang, Z.; Zhang, H. A Flexible Organic Single Crystal with Plastic-Twisting and Elastic-Bending Capabilities and Polarization-Rotation Function. *Angew. Chem.* **2020**, *132*, 13044−13050.

(18) Houjou, H.; Kokubun, M.; Yoshikawa, I.; Araki, K. A High-contrast Dichroic Crystal: A New Metal-containing Tecton with Hybrid Coordination-and Hydrogen-bonding Interactions. *Chem. Lett.* **2009**, *38*, 436−437.

(19) Hara, S.; Houjou, H.; Yoshikawa, I.; Araki, K. Relation between Crystal Packing and Optical Anisotropy for Schiff Base-Nickel Complexes that Form Various Ladder-like Hydrogen-Bonding Networks. *Cryst. Growth Des.* **2011**, *11*, 5113−5121.

(20) Morimoto, K.; Tsujioka, H.; Kitagawa, D.; Kobatake, S. Photoreversible Birefringence Change of Diarylethene Single Crystals

as Revealed by Change in Molecular Polarizability Anisotropy. *J. Phys. Chem. A* **2020**, *124*, 4732−4741.

(21) Carletta, A.; Colaço, M.; Mouchet, S. b. R.; Plas, A. l.; Tumanov, N.; Fusaro, L.; Champagne, B.; Lanners, S.; Wouters, J. Tetraphenylborate Anion Induces Photochromism in N-salicylideneamino-1-alkylpyridinium derivatives through formation of tetra-aryl boxes. *J. Phys. Chem. C* **2018**, *122*, 10999−11007.

(22) Morimoto, M.; Kashihara, R.; Mutoh, K.; Kobayashi, Y.; Abe, J.; Sotome, H.; Ito, S.; Miyasaka, H.; Irie, M. Turn-on mode fluorescence photoswitching of diarylethene single crystals. *CrystEngComm* **2016**, *18*, 7241−7248.

(23) Shoichiro, Y.; Ryutaro, T. Spectrochemical Study of Microscopic Crystals. II. Dichroism of Cobalt (III)-Praseo Salts. *Bull. Chem. Soc. Jpn.* **1952**, *25*, 127−130.

(24) Bushuyev, O. S.; Friščić, T.; Barrett, C. J. Controlling dichroism of molecular crystals by cocrystallization. *Cryst. Growth Des.* **2016**, *16*, 541−545.

(25) Christopherson, J.-C.; Potts, K. P.; Bushuyev, O. S.; Topić, F.; Huskić, I.; Rissanen, K.; Barrett, C. J.; Friščić, T. Assembly and dichroism of a four-component halogen-bonded metal−organic cocrystal salt solvate involving dicyanoaurate (I) acceptors. *Faraday Discuss.* **2017**, *203*, 441−457.

(26) Christopherson, J. C.; Topić, F.; Barrett, C. J.; Friščić, T. Halogen-Bonded Cocrystals as Optical Materials: Next-Generation Control over Light−Matter Interactions. *Cryst. Growth Des.* **2018**, *18*, 1245−1259.

(27) Hutchins, K. M.; Yelgaonkar, S. P.; Harris-Conway, B. L.; Reinheimer, E. W.; MacGillivray, L. R.; Groeneman, R. H. Unlocking pedal motion of the azo group: three- and unexpected eight-component hydrogen-bonded assemblies in co-crystals based on isosteric resorcinols. *Supramol. Chem.* **2018**, *30*, 533−539.

(28) Hutchins, K. M.; Groeneman, R. H.; Reinheimer, E. W.; Swenson, D. C.; MacGillivray, L. R. Achieving dynamic behaviour and thermal expansion in the organic solid state via co-crystallization. *Chem. Sci.* **2015**, *6*, 4717−4722.

(29) Lorenzo, S.; Lewis, G. R.; Dance, I. Supramolecular potentials and embraces for fluorous aromatic molecules. *New J. Chem.* **2000**, *24*, 295−304.

(30) Dance, I.; Scudder, M. Molecules embracing in crystals. *CrystEngComm* **2009**, *11*, 2233−2247.

(31) Campillo-Alvarado, G.; D'mello, K. P.; Swenson, D. C.; Santhana Mariappan, S. V.; Höpfl, H.; Morales-Rojas, H.; MacGillivray, L. R. Exploiting Boron Coordination: B←N Bond Supports a [2 + 2] Photodimerization in the Solid State and Generation of a Diboron Bis-Tweezer for Benzene/Thiophene Separation. *Angew. Chem., Int. Ed.* **2019**, *58*, 5413−5416.

(32) Campillo-Alvarado, G.; D'mello, M. M.; Sinnwell, M. A.; Höpfl, H.; Morales-Rojas, H.; MacGillivray, L. R., Channel Confinement of Aromatic Petrochemicals via Aryl−Perfluoroaryl Interactions With a B←N Host. *Front. Chem.* **2019**, *7*. DOI: 10.3389/fchem.2019.00695

(33) Campillo-Alvarado, G.; Li, C.; Feng, Z.; Hutchins, K. M.; Swenson, D. C.; Höpfl, H.; Morales-Rojas, H.; MacGillivray, L. R. Single-Crystal-to-Single-Crystal [2 + 2] Photodimerization Involving B←N Coordination with Generation of a Thiophene Host. *Organometallics* **2020**, *39*, 2197−2201.

(34) Ray, K. K.; Campillo-Alvarado, G.; Morales-Rojas, H.; Höpfl, H.; MacGillivray, L. R.; Tivanski, A. V. Semiconductor Cocrystals Based on Boron: Generated Electrical Response with $\pi$-Rich Aromatic Molecules. *Cryst. Growth Des.* **2020**, *20*, 3−8.

(35) Campillo-Alvarado, G.; Vargas-Olvera, E. C.; Höpfl, H.; Herrera-España, A. D.; Sánchez-Guadarrama, O.; Morales-Rojas, H.; MacGillivray, L. R.; Rodríguez-Molina, B.; Farfán, N. Self-Assembly of Fluorinated Boronic Esters and 4,4′-Bipyridine into 2:1 N→B Adducts and Inclusion of Aromatic Guest Molecules in the Solid State: Application for the Separation of *o,m,p*-Xylene. *Cryst. Growth Des.* **2018**, *18*, 2726−2743.

(36) Fornasari, L.; Mazzaro, R.; Boanini, E.; d'Agostino, S.; Bergamini, G.; Grepioni, F.; Braga, D. Self-Assembly and Exfoliation of a Molecular Solid Based on Cooperative B−N and Hydrogen Bonds. *Cryst. Growth Des.* **2018**, *18*, 7259−7263.

(37) Stephens, A. J.; Scopelliti, R.; Tirani, F. F.; Solari, E.; Severin, K. Crystalline Polymers Based on Dative Boron−Nitrogen Bonds and the Quest for Porosity. *ACS Mater. Lett.* **2019**, *1*, 3−7.

(38) Campillo-Alvarado, G.; MacGillivray, L. R. Opportunities Using Boron to Direct Reactivity in the Organic Solid State. *Synlett* **2021**, *32*, 655.

(39) Körte, L. A.; Schwabedissen, J.; Soffner, M.; Blomeyer, S.; Reuter, C. G.; Vishnevskiy, Y. V.; Neumann, B.; Stammler, H.-G.; Mitzel, N. W. Tris(perfluorotolyl)borane—A Boron Lewis Superacid. *Angew. Chem., Int. Ed.* **2017**, *56*, 8578−8582.

(40) Lesley, M. G.; Woodward, A.; Taylor, N. J.; Marder, T. B.; Cazenobe, I.; Ledoux, I.; Zyss, J.; Thornton, A.; Bruce, D. W.; Kakkar, A. K. Lewis acidic borane adducts of pyridines and stilbazoles for nonlinear optics. *Chem. Mater.* **1998**, *10*, 1355−1365.

(41) Höpfl, H. The tetrahedral character of the boron atom newly defined—a useful tool to evaluate the N→ B bond. *J. Organomet. Chem.* **1999**, *581*, 129−149.

(42) Sasaki, T.; Miyata, M.; Tsuzuki, S.; Sato, H. Experimental and Theoretical Analysis of Two-Fold Helix-Based Chiral Crystallization by Confined Interhelical CH/$\pi$ Contacts. *Cryst. Growth Des.* **2019**, *19*, 1411−1417.

(43) Maleki, A.; Seidali, Z.; Zakerhamidi, M. S.; Ara, M. H. M. Dichroic ratio and order parameters of some Sudan dyes doped in nematic liquid crystalline matrix. *Optik* **2015**, *126*, 5473−5477.

(44) Spackman, M. A.; Jayatilaka, D. Hirshfeld surface analysis. *CrystEngComm* **2009**, *11*, 19−32.

(45) McKinnon, J. J.; Jayatilaka, D.; Spackman, M. A. Towards quantitative analysis of intermolecular interactions with Hirshfeld surfaces. *Chem. Commun.* **2007**, 3814−3816.

(46) Jaime-Adán, E.; Germán-Acacio, J. M.; Toscano, R. A.; Hernández-Ortega, S.; Valdés-Martínez, J. Imine-Benzoic Acid Cocrystals as a Tool to Study Intermolecular Interactions in Schiff Bases. *Cryst. Growth Des.* **2020**, *20*, 2240−2250.

(47) Crystal Data for (**BCF**)·(**4PAzP**) ($M$ = 1390.40 g/mol): monoclinic, space group $P2_1/c$ (No. 14), $a$ = 23.2264(8) Å, $b$ = 17.6402(6) Å, $c$ = 13.6898(5) Å, $\beta$ = 106.106(1)°, $V$ = 5388.8(3) Å$^3$, $Z$ = 4, $T$ = 100.0 K, $\mu$(CuK$\alpha$) = 1.580 mm$^{-1}$, $D_{calc}$ = 1.714 g/cm$^3$, 153 468 reflections measured (6.386° ≤ 2Θ ≤ 144.284°), 10 606 unique ($R_{int}$ = 0.0395, $R_{sigma}$ = 0.0178), which were used in all calculations. The final $R_1$ was 0.0288 ($I > 2\sigma(I)$), and $wR_2$ was 0.0774 (all data).



https://doi.org/10.1021/acs.cgd.1c00114
*Cryst. Growth Des.* XXXX, XXX, XXX−XXX